Force fluctuations and polymerization dynamics of intracellular microtubules

Clifford P. Brangwynne[†‡], F. C. MacKintosh[§], and David A. Weitz[†¶‖]

[†]School of Engineering and Applied Sciences, Harvard University, Cambridge, MA 02138; [§]Department of Physics and Astronomy, Vrije Universiteit, 1081 HV, Amsterdam, The Netherlands; and [¶]Department of Physics, Harvard University, Cambridge, MA 02138

Edited by Tom C. Lubensky, University of Pennsylvania, Philadelphia, PA, and approved August 16, 2007 (received for review April 3, 2007)

Microtubules are highly dynamic biopolymer filaments involved in a wide variety of biological processes including cell division, migration, and intracellular transport. Microtubules are very rigid and form a stiff structural scaffold that resists deformation. However, despite their rigidity, inside of cells they typically exhibit significant bends on all length scales. Here, we investigate the origin of these bends using a Fourier analysis approach to quantify their length and time dependence. We show that, in cultured animal cells, bending is suppressed by the surrounding elastic cytoskeleton, and even large intracellular forces only cause significant bending fluctuations on short length scales. However, these lateral bending fluctuations also naturally cause fluctuations in the orientation of the microtubule tip. During growth, these tip fluctuations lead to microtubule bends that are frozen-in by the surrounding elastic network. This results in a persistent random walk of the microtubule, with a small apparent persistence length of ≈30 μm, ≈100 times smaller than that resulting from thermal fluctuations alone. Thus, large nonthermal forces govern the growth of microtubules and can explain the highly curved shapes observed in the microtubule cytoskeleton of living cells.

cytoskeleton | mechanics | nonequilibrium | persistence length | rigidity

Microtubules are biopolymer filaments that are essential for many fundamental biological processes including cell division, migration, and transport. Microtubules exhibit highly dynamic growth behavior, with repeated cycles of polymerization and depolymerization (1), allowing the microtubule network to rapidly restructure to perform different tasks. Many of these tasks require the network to behave as a rigid scaffold that can support mechanical loads, such as those generated by motors during cargo transport. Mechanical stability of microtubules is also crucial in guiding directional cell migration and effectively connecting to and pulling apart chromosomes during mitosis. Indeed, each of their varied biological roles requires some degree of mechanical stability. Consistent with this, microtubules are the most rigid of the cytoskeletal filaments; they are ≈100 times more resistant to bending than actin filaments. As a result of this high bending rigidity, microtubule shapes are relatively insensitive to thermal Brownian forces: *in vitro* experiments with isolated microtubules show that they exhibit significant thermal bending fluctuations only beyond a length scale on the order of a few millimeters, known as the persistence length (2). This persistence length is 10–100 times larger than a typical animal cell, which suggests that Brownian fluctuations do not contribute to microtubule bending in cells.

Although microtubules are sufficiently stiff to resist small thermal fluctuations, inside of animal cells they can also experience large, nonthermal forces such as those arising from myosin contractility (3) or other ATP-consuming motor proteins. Indeed, in most adherent cells, microtubules exhibit significant curvature on both short and long length scales, as shown in Fig. 1*a*. Such bends are ubiquitous in animal cells, and are generally thought to arise after growth, by bending under the action of internal cytoskeletal forces, as shown schematically in Fig. 1*a Inset* (3, 4). However, the surrounding elastic cytoskeleton has been shown to mechanically reinforce microtubules to withstand these large forces; this suppresses bending, particularly on long length scales (5). As a result, under the action of even large nonthermal forces, bending occurs primarily on short wavelengths of ≈3 μm. Such dynamic, short-wavelength bends can be observed to fully fluctuate in time, as shown in the temporal sequence of the shape of a single microtubule in a GFP-tubulin-transfected CHO cell, Fig. 1*b* [also see supporting information (SI) Movie 1]. Bending on longer wavelengths may result from slow, large-scale cellular restructuring, such as that occurring because of the retrograde flow of the entire cytoskeletal network at the leading edge of cells (3). These microtubule bends will significantly affect the location of the distal tips of growing microtubules and therefore affect their well known role in targeting and biochemical signaling (6, 7), in addition to the myriad biological processes that depend on the overall structure of the microtubule network. However, although the architecture of the microtubule network is of central biological importance, the precise origin of microtubule bending and the role of mechanical forces in establishing this network architecture remain unclear.

In this article, we show that large-scale microtubule bends result primarily from the coupling of active intracellular forces to the dynamics of microtubule growth; this leads to a dramatically reduced persistence of directional growth. During microtubule growth, nonthermal forces cause directional reorientation of microtubule tips. As a microtubule grows under the action of these fluctuating forces, its growth trajectory is curved, and the resulting microtubule bends are locked in by the surrounding cytoskeletal network. As we show, the fluctuations in tip orientation suggest a persistent random walk trajectory of microtubule growth, in agreement with the microtubule shapes we observe. However, the apparent persistence length observed is ≈100 times smaller than the thermal persistence length. Moreover, once a microtubule is grown, the surrounding elastic network reinforces it against bending under the action of these forces. Large nonthermal force fluctuations thus appear to play a central role in establishing the structure of the microtubule network, primarily by affecting the directionality of microtubule growth; these fluctuations also are likely to affect a number of other microtubule-associated processes such as the generation of polymerization forces and intracellular transport.

Results

Fourier Analysis of Intracellular Microtubules Shapes. ***Anomalous distribution of instantaneous bends.*** To quantitatively investigate the origin of microtubule bending in cells, we used automated contour

Author contributions: C.P.B., F.C.M., and D.A.W. designed research; C.P.B. performed research; C.P.B. and F.C.M. contributed new reagents/analytic tools; C.P.B. analyzed data; and C.P.B., F.C.M., and D.A.W. wrote the paper.

The authors declare no conflict of interest.

This article is a PNAS Direct Submission.

[‡]Present address: Max Planck Institute of Molecular Cell Biology and Genetics, Pfotenhauerstrasse 108, 01307 Dresden, Germany.

[‖]To whom correspondence should be addressed at: Harvard University, 29 Oxford Street, Pierce 231, Cambridge, MA 02138. E-mail: weitz@seas.harvard.edu.

This article contains supporting information online at www.pnas.org/cgi/content/full/0703094104/DC1.

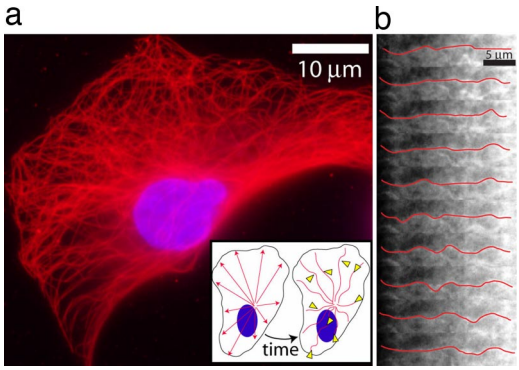

Fig. 1. Microtubule bending in cells. (*a*) A fixed CHO cell, stained for microtubules (red) and the nucleus (blue), showing highly bent microtubules throughout the cell. (*Inset*) Schematic showing that microtubules are believed to grow fairly straight and subsequently become bent under the action of intracellular forces (yellow arrowheads). (*b*) Microtubules undergo significant bending fluctuations in time, as seen by the microtubule highlighted in this GFP-tubulin-transfected CHO cell. Consecutive images are separated by 8 sec ($t = 0$ at top).

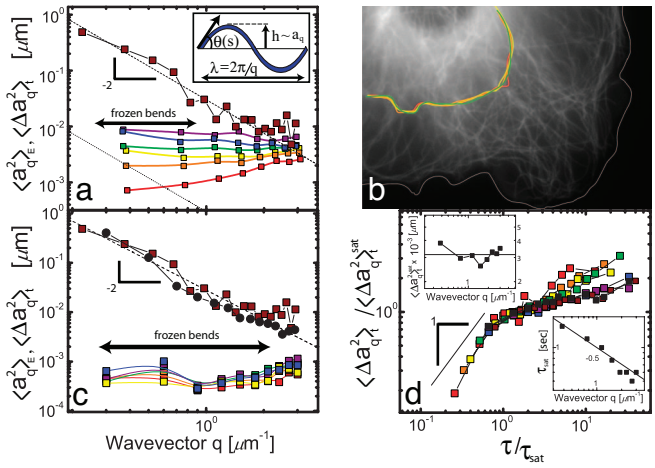

Fig. 2. Fourier analysis of microtubule bends. (*a*) The ensemble variance of Fourier amplitudes obtained from fixed CHO cells is shown in the brown squares and exhibits a thermal-like q-dependence: $\langle a_q^2 \rangle_E = \frac{1}{l_p^*} \cdot \frac{1}{q^2}$ with $l_p^* \sim 30$ μm. The lower dotted line indicates the expected variance of a thermally fluctuating filament, with $l_p \sim 3$ mm. The lower colored curves indicate the magnitude of amplitude fluctuations, $\langle \Delta a_q^2(\tau) \rangle_t$, for different lag times. Red, orange, yellow, green, blue, and purple correspond to $\tau = 0.4$, 0.8, 1.6, 4, 8, and 20 sec, respectively. (*b*) This is visible in movies of fluctuating microtubules in GFP-tubulin COS-7 cells. A single long microtubule is highlighted: red, orange, yellow, and green contours correspond to $t = 0$, 8, 16, and 24 sec, respectively. (*c*) In ATP-depleted CHO cells, the instantaneous Fourier bending spectrum (black circles) is similar to that of control cells (brown squares). However, there are no fluctuations in time, and bends are locked-in on all wavelengths. Red, orange, yellow, green, blue, and purple correspond to $\tau = 2$, 10, 20, 40, 70, and 100 sec, respectively. (*d*) Time dependence of the fluctuations in Fourier amplitude for different q, where red, orange, yellow, green, blue, purple, brown, and black correspond to $q \cong 0.4$, 0.75, 1.1, 1.5, 1.9, 2.25, 2.6, and 3.0 μm^{-1}, respectively; the data were scaled together by dividing each curve by its apparent saturation, $\langle \Delta a_q^2(\tau) \rangle_t^{sat}$, whose values are shown in the upper *Inset*, and by dividing the lag time by the time scale at which the fluctuations appear to become sublinear, τ_{sat}, whose values are shown in the lower *Inset*.

tracking algorithms to trace the shapes of fluorescently labeled microtubules (8). From the instantaneous contours, we determine the local tangent angle $\theta(s)$ of each microtubule as a function of the contour length s along the microtubule. The shape is then decomposed into component Fourier modes (2) by expressing $\theta(s)$ as a sum of cosines:

$$\theta(s) = \sqrt{\frac{2}{L}} \sum_{n=0}^{\infty} a_q \cos(qs).$$

Here, L is the total filament length, and $q = n\pi/L$ is the wave vector. This technique allows us to determine the amplitude of bending as a function of the length scale over which the bending occurs. The bending amplitude is given by the Fourier amplitude a_q, which is proportional to the height of a bend on a wavelength, $\lambda = 2\pi/q$, as illustrated in Fig. 2*a Inset*. The $n = 0$ mode corresponds to a constant angle and therefore accounts for the average orientation of the microtubule. The $n = 1$ mode corresponds to a smooth curvature in only one direction, whereas a full wavelength bend is given by the $n = 2$ mode. Each of the amplitudes a_q for a single microtubule depends on time because the shape $\theta(s)$ changes with time.

For microtubules in thermal equilibrium, the square of the amplitude, averaged over uncorrelated microtubule shapes, is given by

$$\langle a_q^2 \rangle = \frac{1}{l_p} \cdot \frac{1}{q^2},$$

where l_p is the persistence length, whose value is on the order of several millimeters (2); the angle brackets indicate an average, which can be a time average, over uncorrelated shapes of a single, unconstrained microtubule at different times, or an ensemble average, over many different filaments. For intracellular filaments, we can determine an ensemble-averaged variance by analyzing the instantaneous shapes of many different microtubules in fixed animal cells. We find that the q-dependence of the Fourier bending spectrum is given by

$$\langle a_q^2 \rangle_E = \frac{1}{l_p^*} \cdot \frac{1}{q^2},$$

where the subscript emphasizes the ensemble average; this is shown for microtubules in CHO cells by the brown squares in Fig. 2*a*. This yields an apparent persistence length, $l_p^* \sim 30$ μm, that is $\approx$100 times smaller than expected from thermal fluctuations alone, indicating significantly larger amplitude bending fluctuations. The Fourier bending spectrum of microtubules in COS-7 cells exhibits similar behavior. This unexpectedly large amplitude of bending suggests a nonthermal origin.

Whereas the enhanced fluctuation in cells, relative to thermal equilibrium, is itself not surprising, the observed thermal-like wave vector dependence, $\langle a_q^2 \rangle_E \sim q^{-2}$, is surprising because there is no reason to expect *a priori* that cellular or motor activity within the composite cytoskeleton should lead to an equilibrium-like distribution of bending amplitudes. In fact, even if the cellular activity were random and characterized by an elevated effective temperature, the $\langle a_q^2 \rangle_E \sim q^{-2}$ would not be expected because, unlike a free microtubule in buffer, the energy of microtubule bending is determined not only by bending rigidity but also by the elasticity of the surrounding matrix.

Time-dependent bending fluctuations. To investigate the origin of these anomalous bending amplitudes, and the role of cellular activity, we tracked the time-dependent bending fluctuations of microtubules in living cells transfected with GFP-tubulin. This is illustrated by comparing subsequent shapes of a single microtubule in a GFP-tubulin-transfected COS-7 cell, as indicated by the contours of a single microtubule in Fig. 2*b*, where each color represents the contour at a different time separated by 8 sec. The Fourier amplitudes of each individual filament were determined for each

point in time, and the average of fluctuations over time was calculated from the mean-squared amplitude difference as a function of lag time, $\langle \Delta a_q^2(\tau)\rangle_t = \frac{1}{2}\langle (a_q(t+\tau) - a_q(t))^2\rangle_t$, where the angle brackets indicate an average over all initial times, t, and the subscript t emphasizes that this is a time average of individual filaments. For long lag times τ, we expect the shapes of an individual microtubule to be uncorrelated, from which it follows that $\langle \Delta a_q^2(\tau)\rangle_t \rightarrow \langle a_q^2\rangle_t$. For a collection of identical, freely fluctuating filaments, this would be equal to the ensemble-averaged variance, $\langle a_q^2\rangle_E$. We find that within ≈10 sec, short-wavelength ($\lambda \leq 6$ μm, or $q \geq 1$ μm^{-1}) microtubule bends behave in this way: time- and ensemble-averaged variances are approximately equal. By contrast, however, the average fluctuations of the long-wavelength bends (small wave vectors) do not appear to fully reach ensemble-averaged values, suggesting that they are constrained by the surrounding matrix; this behavior is shown by the colored curves in Fig. 2*a*, where each color represents a different lag time, τ. In fact, we find that although the mode amplitudes initially fluctuate roughly linearly in time, $\langle \Delta a_q^2(\tau)\rangle_t \sim \tau$, this initial diffusive-like motion gives way to an apparent second stage of much slower evolution, consistent with the constraint of the surrounding cytoskeleton, as shown in Fig. 2*d*. The latter appears to dominate for larger wavelengths or smaller wave vectors q. As a result of this slow evolution, a bend on a length scale of ≈10 μm would require ≈1,000 sec to fully fluctuate, which is longer than the lifetime of a typical microtubule (9). Such constrained or frozen-in long-wavelength microtubule bends can, in fact, be directly observed in the example highlighted in Fig. 2*b*, where the filament undergoes highly dynamic short-wavelength fluctuations while the long-wavelength arc is maintained. Thus, whereas instantaneous microtubule bends have a thermal-like $\langle a_q^2\rangle_E \sim q^{-2}$ dependence, long-wavelength bends appear to fluctuate very little in time.

Lateral Fluctuations Have a Nonthermal Origin. To elucidate the origin of the forces that drive the microtubule bending dynamics, we depleted cells of ATP, which will limit any mechanochemical enzymatic activity, such as that of myosin and other motors. ATP depletion has been shown to have only a small effect on the mechanical properties of the cytoskeleton (10) and should not change the magnitude of thermally driven microtubule bending fluctuations. We fixed and stained ATP-depleted CHO cells and analyzed the instantaneous ensemble microtubule shapes, as above. We find that, once they have formed, the presence of these microtubule bends does not depend on ATP, and the ensemble variance is similar to that of control cells. However, the time-dependent fluctuations of these bends are completely arrested, as shown in Fig. 2*c*. The instantaneous bends do not evolve in time and are completely frozen-in on all length scales. Thus, the ATP dependence of short-wavelength bending dynamics suggests that these fluctuations have a distinctly nonthermal origin, consistent with recent studies of the dynamics of motor-driven force fluctuations in the cytoskeleton (10–12).

Role of Microtubule Growth in Establishing Shape. ***Force-induced redirection of microtubule growth.*** Given the very slow evolution of the long-wavelength bending modes, it is unlikely that these bending fluctuations can account for the development of a network of highly bent microtubules, starting from initially straight filaments. Rather, we hypothesize that the observed spectrum of bent shapes in Fig. 2*a* results from curved growth trajectories of microtubule tips, possibly because of the action of fluctuating internal cytoskeletal forces. These active forces not only will lead to lateral microtubule bending fluctuations but also will naturally cause directional reorientation of the microtubule tip, as shown schematically in Fig. 3*a*. Furthermore, as we show, such orientational fluctuations would naturally lead to the $\langle a_q^2\rangle_E \sim q^{-2}$ dependence of the ensemble average that we observe for microtubule shapes.

To test the hypothesis that lateral bending forces can reorient the microtubule tip, we used a microneedle to apply a transverse force to the region behind a growing microtubule tip (Fig. 3*b*). Microtubule growth could indeed be redirected under the action of such an exogenous force, as shown by the change in direction of the tip of a microtubule highlighted in red in Fig. 3*c* (also see SI Movie 2). Intrinsic cytoskeletal forces appear capable of redirecting microtubule growth in a similar manner, because microtubules frequently appear to change their direction of growth in response to local bending forces, as shown by the growing microtubule highlighted in red in Fig. 3*d* (also see SI Movie 3). Moreover, such naturally redirected microtubules give rise to relatively static, long-wavelength bends, as can be seen in the example in Fig. 3*d*.

Analysis of microtubule growth trajectories. Force-induced tip deflections provide a quantitative explanation for the wavelength dependence of the large bending amplitudes shown in Fig. 2*a*. Specifically, given the elastic environment in which a microtubule grows, lateral forces will lead to directional reorientation that can persist; the resultant directional fluctuations become independent over a distance on the order of a few micrometers. In such a growth process, the tip, defined by position s', has an orientation $\theta(s')$, which performs a random walk, with $\langle(\theta(s') - \theta(0))^2\rangle = 2D_\theta s'$; this results in a spectrum of the form $\langle a_q^2\rangle_E \sim q^{-2}$.

To quantitatively test this hypothesis, we analyze the motion of microtubule tips using CHO cells expressing YFP CLIP-170, a protein that specifically associates with the tips of growing microtubules (13). We tracked the position of microtubule tips in these cells and measured their lateral fluctuations by fitting a short segment of the growth trajectory to a line and determining the deviation from this line as a function of time, $h(t)$. We find that microtubule tips undergo significant lateral fluctuations as a function of time, as shown by the plot of $h(t)$ for a microtubule tip in the upper *Inset* of Fig. 3*e* (also see SI Movies 4 and 5). These tip fluctuations are qualitatively similar to the lateral bending fluctuations along the microtubule backbone, as shown by the plot of the time dependence of a Fourier amplitude, a_q, in the lower *Inset* of Fig. 3*e* . Moreover, both tip fluctuations and lateral microtubule bending fluctuations exhibit a diffusive character, as shown by the roughly linear τ-dependence of the mean-squared displacement of the lateral deviation, $\langle(h(t+\tau) - h(t))^2\rangle_t$ (green triangles), and the example of a mean-squared difference of Fourier amplitude, $\langle \Delta a_q^2(\tau)\rangle_t$ (blue squares), in Fig. 3*e*. This suggests that force-induced lateral microtubule bending fluctuations are indeed associated with microtubule tip fluctuations. Because these forces are sustained over a period of several seconds, the microtubule will continue to grow in the new direction defined by the reoriented microtubule tip, and the resulting bend will be stabilized by the surrounding elastic network. Consistent with this, the trajectories of growing microtubules revealed by an overlay of successive positions of YFP CLIP-170-labeled microtubule tips shows that tip trajectories frequently exhibit significant curvature, as shown by the microtubule trajectories highlighted in red in Fig. 3*f Inset*; this suggests that such behavior is quite general.

To further test this physical picture, we performed a Fourier analysis of the trajectories of hundreds of growing microtubule tips in YFP CLIP-170-expressing CHO cells. As predicted by the tip-reorientation mechanism, these growth trajectories exhibit a roughly $\langle a_q^2\rangle_E \sim q^{-2}$ ensemble-averaged Fourier spectrum, as shown by the yellow squares in Fig. 3*f*. Further confirmation comes from the fact that this curve is nearly identical to the ensemble-averaged variance of grown microtubules (brown squares in Fig. 3*f*), strongly suggesting that these curved microtubule growth trajectories are indeed the origin of the locked-in long-wavelength bends.

Newly grown microtubules are highly bent. If tip fluctuations during growth give rise to the thermal-like Fourier bending spectrum of intracellular microtubules, $\langle a_q^2\rangle_E \sim q^{-2}$, this Fourier spectrum should be apparent even in newly grown microtubules that have not had time to undergo significant lateral bending fluctuations. To test this, we depolymerized microtubules by treating COS-7 cells with

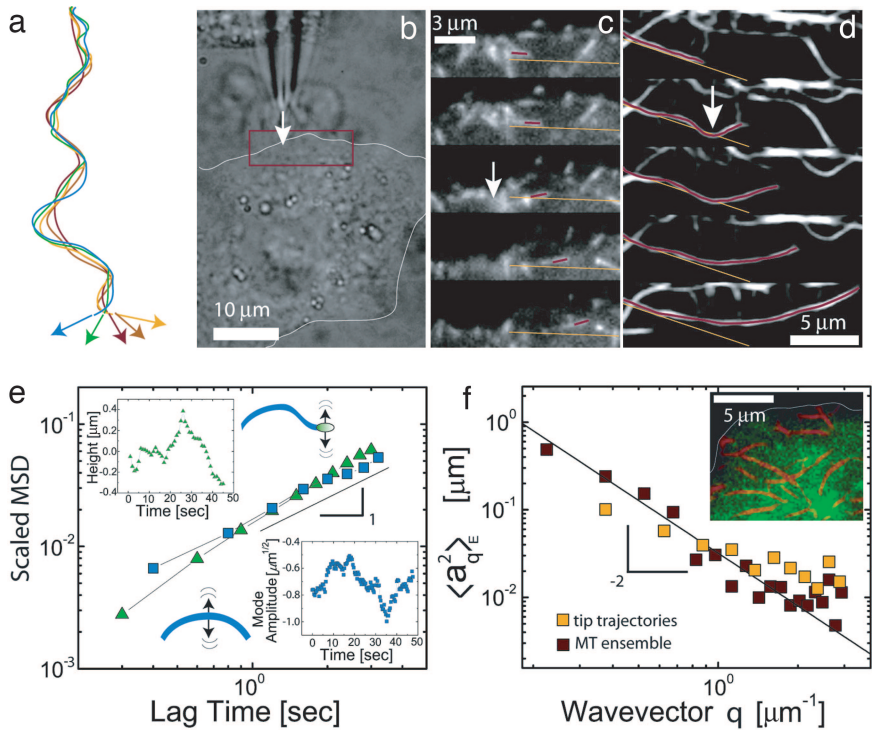

Fig. 3. Lateral bending forces induce tip reorientation. (*a*) Schematic illustration showing that lateral bending fluctuations of a microtubule naturally lead to fluctuations in the orientation of the tip. Each color indicates the contour at a different time, and the arrows indicate the corresponding directional orientation of the tip. (*b*) Phase contrast image of a CHO cell. For clarity, the cell outline is indicated by the white line. A microneedle that will be moved down to apply a force to the edge of the cell (arrow) is visible in the top of the image. (*c*) Fluorescence images in which YFP CLIP-170 microtubule tips are visible within the CHO cell shown in *b*; the region corresponds to the red-boxed region in *b*. For the first two frames, the microtubule tip highlighted in red is growing to the right, with a roughly horizontal orientation indicated by the yellow line. At the third frame, the microneedle is pushed into the region immediately behind this growing microtubule tip; the location is indicated by the arrow. As a result of this exogenous force, the microtubule tip is redirected upward, and it continues growing in that direction. Frame times are 0, 3, 8, 16, and 29 sec from the top to the bottom. (*d*) A microtubule within a GFP-tubulin-transfected COS-7 cell, highlighted in red, can be seen growing toward the lower right in the direction indicated by the yellow line. In the second frame, the filament experiences a naturally occurring bending fluctuation due to internal forces, as indicated by the arrow. As a result, the orientation of the microtubule tip changes, and the microtubule grows upward, giving rise to a long-wavelength bend. The frame times are 0, 36, 46, 53, and 92 sec from the top to the bottom. Deviation from a straight line as a function of time for a microtubule tip is shown by the green triangles in the upper *Inset* of *e*. The mean-squared displacement (MSD) is approximately linear, as shown by the green triangles in *e*. The time dependence of a Fourier bending amplitude from a microtubule in a CHO cell ($q = 1.06\ \mu m^{-1}$) is shown by the blue squares in the lower *Inset* of *e*. The mean-squared difference in amplitude is also approximately linear, as shown by the blue squares in *e*. The curves are arbitrarily shifted in the vertical direction for comparison. The upper *Inset* in *f* shows a maximum intensity projection of CLIP-170 microtubule tip positions (red) over the course of 100 sec, showing significantly bent growth trajectories. The Fourier spectrum of these tip trajectories (yellow squares in *f*) is in close agreement with the $\langle a_q^2 \rangle_E \sim q^{-2}$ Fourier spectrum of bends present in already grown microtubules (brown squares in *f*).

nocodazole for 6–8 h, after which there are no microtubules detected (upper *Inset* in Fig. 4*a*). The cells remain alive and well spread, although their morphology is slightly altered. These microtubule-free cells were then washed to remove nocodazole, and after only 5 min the cells were fixed and stained for tubulin. By then, many microtubules have begun to regrow in these cells, as shown in Fig. 4*a*. These newly grown microtubules are already highly bent, as shown in the higher-magnification view in Fig. 4*b*. Moreover, their Fourier spectrum is indistinguishable from that of microtubules in control cells, as shown in Fig. 4*c*. Thus, microtubules assume a highly bent shape, with an approximately q^{-2}-dependent mode spectrum, in <5 min of growth.

Discussion

Intracellular microtubules play a wide variety of fundamental biological roles. In addition to functioning as a mechanochemical scaffold controlling cell shape, microtubules also guide polarized cell migration, act as a highway system for motor-driven transport, and mediate the controlled distribution of DNA and other material between daughter cells.

To perform these varied tasks, microtubules continually restructure, undergoing repeated cycles of growth and depolymerization (1). This dynamic instability is particularly well suited for restructuring into different functional microtubule network architectures because microtubules that fail to grow into a proper location can simply depolymerize over much of their length and then regrow along different trajectories into a new region of the cell, repeating the process until stabilized upon growth into an appropriate region. This has been termed "search and capture" (14) and may constitute a generic mechanism for self-assembly of functional microtubule networks by selection and stabilization. Growth along different trajectories is clearly necessary for such a mechanism because if a microtubule repeatedly grows along the same straight path, very little of the cell is explored. This could be accomplished by complete depolymerization of the microtubule back to its origin, followed by regrowth from a nucleation site with a different orientation. However, in animal cells, most microtubules exhibit "recovery" from shrinkage well before full depolymerization, with the same microtubule undergoing repeated shrinking and regrowth into the leading edge. Under the action of only small thermal fluctuations, a microtubule that undergoes such recovery would simply regrow into the same small area of the cell. Indeed, although dynamic instability is particularly well suited to restructuring and self-assembly of the microtubule network, the high rigidity of microtubules would tend to limit such network plasticity. However, in the presence of large, fluctuating nonthermal forces, the resulting tip fluctuations will lead to a dramatic reorientation upon regrowth, and the tip will explore a much broader region of the cell. To illustrate this, we generate growth trajectories using a simple two-dimensional simulation in which a filament begins with a horizontal orientation, growing toward the right. At each time step, the filament tip, at position s', extends by an amount Δs, and its orientation receives a small random perturbation $\delta\theta$, such that the new tip orientation is given by $\theta(s' + \Delta s) = \theta(s') + \delta\theta$. Under purely thermal fluctuations, $\delta\theta$ is small, and the filaments naturally grow into nearly straight trajectories, as shown by the blue curves in Fig. 5*a*. Thus, a microtubule "searching" under the action of thermal fluctuations alone will only explore the small sliver of the cell traversed by these blue filaments. However, under the action of larger nonthermal fluctuations, this "searching" ability of microtubules changes dramatically. When the magnitude of the fluctuations, $\sqrt{\langle \delta\theta^2 \rangle}$, is increased by a factor of 10, the trajectories exhibit significant curvature, as shown by the red curves in Fig. 5*a*. These simulated trajectories exhibit remarkable qualitative similarity with

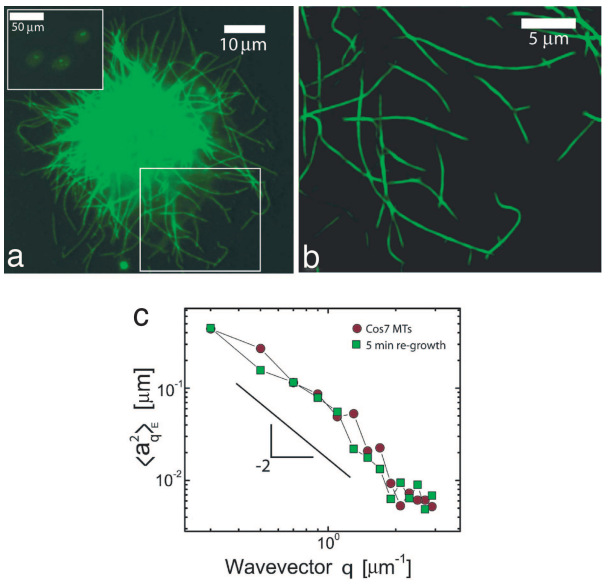

Fig. 4. Fourier bending spectrum of newly grown microtubules. The upper *Inset* in *a* shows COS-7 cells after an 8-h incubation with nocodazole, at which point no microtubules are detected by immunofluorescence staining. After only 5 min of incubation in fresh nocodazole-free media, many microtubules have begun growing, as shown in *a*. (*b*) High-resolution view of the lower boxed region in *a*, showing highly bent microtubules. (*c*) The Fourier spectrum of microtubules after only 5 min of growth (green squares) is identical to that of untreated control cells (red circles), exhibiting the form $\langle a_q^2 \rangle_E \sim q^{-2}$.

the actual trajectories obtained from tracking the tips of microtubules in CHO cells, as shown in Fig. 5*b*. Moreover, simulated trajectories also exhibit a Fourier bending spectrum of $\langle a_q^2 \rangle_E \sim \frac{1}{l_p^*} \cdot \frac{1}{q^2}$, where $l_p^* \sim \langle \delta\theta^2 \rangle^{-1}$.

We have shown that nonthermal force fluctuations lead to significant microtubule curvature in cells, primarily by causing curved growth trajectories. As a result, microtubules exhibit a persistent random walk trajectory, with an apparent persistence length, l_p^*, ≈100 times less than that of microtubules *in vitro*. However, it is important to note that although nonthermal forces cause microtubules to exhibit a small apparent persistence length, their actual rigidity need not be small. Although it is possible that the small apparent persistence length could arise if intracellular microtubules are significantly softer than *in vitro*, *in vitro* measurements under a variety of conditions, including with and without microtubule associated proteins, have shown that the rigidity of microtubules varies by at most an order of magnitude (8, 15, 16). Moreover, the lateral bending fluctuations are strongly ATP-dependent, and thus thermal fluctuations alone cannot be responsible. Another possible contribution to the small apparent persistence length is defects in the microtubule lattice that could cause locked-in bends ("kinks") during growth. However, the nature of tip reorientation events (e.g., Fig. 3*d*) appears to be inconsistent with a lattice defect mechanism. This could conceivably be tested by removing the surrounding cytoskeleton, although complete cytoskeletal disruption typically results in pathological features such as blebbing and cell retraction. Nevertheless, our results suggest that tip reorientation from force fluctuations alone is sufficient to explain the small apparent persistence length. Indeed, using the approximate mechanical properties of the cytoskeleton, we estimate that the observed persistence length, l_p^*, of order 10 μm, can arise from nonthermal forces of order 1–10 pN, comparable with forces generated by individual motor proteins (see *SI Text* and SI Fig. 6).

In addition to dramatically increasing the effective plasticity of the microtubule network, fluctuating nonthermal forces also have important implications for force generation by polymerization. Growing microtubules are known to be capable of generating mechanical forces that are important for movement within cells (17). This is typically explained by the Brownian ratchet mechanism, whereby the chemical energy of polymerization is converted into directional force generation through harnessed fluctuations, typically assumed to be of a thermal nature (18, 19). *In vitro* experiments on thermally fluctuating microtubules have shown this to be an adequate description of the piconewton-level forces generated when a microtubule polymerizes against a wall (16). Polymerization forces *in vivo* are usually assumed to also be driven

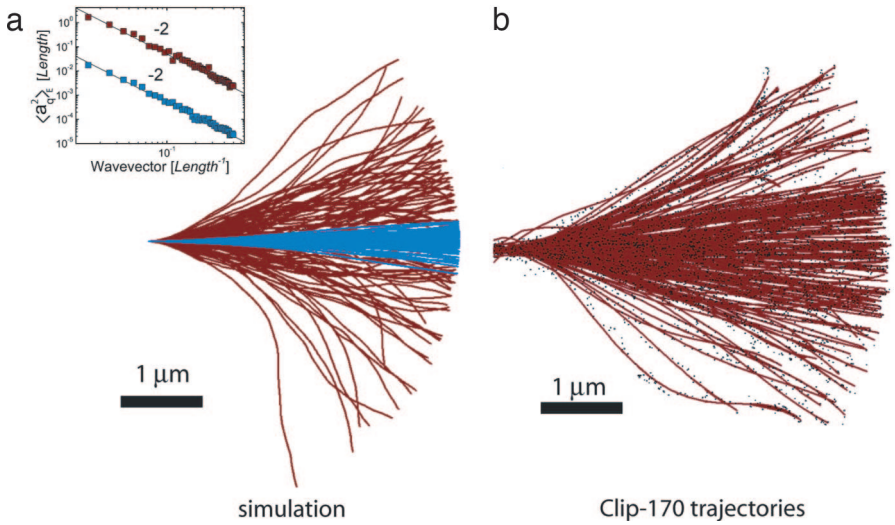

Fig. 5. Simulated and real microtubule trajectories. (*a*) Filament growth was simulated as described in the text. Shown in blue is an ensemble of filaments that exhibit a very large persistence length similar to that of thermally fluctuating microtubules (≈1 mm); as a result, they can explore only the small blue sliver indicated. By increasing the lateral fluctuations, $\sqrt{\langle \delta\theta^2 \rangle}$, by a factor of 10, the filaments exhibit significantly larger bending (red filaments) and can thus explore a correspondingly large region of the cell. The Fourier bending spectrum of these two ensembles of filaments are shown in the upper *Inset* and exhibit the form $\langle a_q^2 \rangle_E \sim q^{-2}$. (*b*) As with the simulation under large fluctuations, real intracellular CLIP-170 microtubule growth trajectories are also highly bent and exhibit remarkable qualitative similarity.

by thermal fluctuations, although neither forces nor fluctuations have been directly measured for intracellular microtubules. Because nonthermal fluctuations are clearly important in causing fluctuations in microtubule tips, they may therefore also be the dominant factor in determining the magnitude of polymerization forces generated in cells. These fluctuations are much larger than thermal fluctuations, and the resulting polymerization forces will be correspondingly larger.

Conclusions

We have shown that microtubules in adherent animal cells have a surprisingly thermal-like bending spectrum, with bends on both long and short wavelengths. However, only short-wavelength bends fluctuate significantly in time, whereas long-wavelength bends are effectively frozen-in. These fluctuations result from active, nonthermal forces within cells and lead to an apparent persistence length that is ≈100 times smaller than the thermal persistence length measured *in vitro*. This small apparent persistence length arises during growth, when active forces cause fluctuations in the orientation of growing microtubule tips, leading to long-wavelength bends that are subsequently frozen-in by the surrounding elastic network. Thus, microtubules are at once highly rigid biopolymers that are further reinforced by the surrounding network while at the same time being highly deformable under the action of large forces during growth. This has important implications for the mechanical properties and behavior of the microtubule cytoskeleton, including microtubule targeting processes and force generation by polymerization.

Materials and Methods

Cell Culture. COS-7 cells (African green monkey kidney-derived) were obtained from American Type Culture Collection and cultured in 10% FBS DMEM. YFP CLIP-170 CHO cells (a kind gift of Yulia Komarova, University of Illinois at Chicago) were cultured in 10% FBS DMEM without glucose and sodium pyruvate. For visualization of static microtubule shapes, cells were fixed in 0.25% glutaraldehyde/0.5% Triton X-100 for 1 min, followed by 1% glutaraldehyde for 10 min. Cells were then stained with a mouse anti-α-tubulin primary antibody DMIA, followed by rhodamine-conjugated anti-mouse IgG (both from Calbiochem), using standard procedures. For studies of the dynamics of intracellular microtubules, confluent monolayers of cells were incubated for 24–48 h with an adenoviral vector encoding EGFP-tubulin (5). Cells were sparsely plated onto glass-bottomed 35-mm dishes (MatTek) and allowed to adhere and spread overnight. For ATP-depletion studies, cells were incubated in 2 mM sodium azide/10 mM deoxyglucose in phosphate-buffered saline for 30 min.

Microscopy. All images were acquired on a Leica DM-IRB epifluorescence microscope equipped with a heated stage to maintain cells at a temperature of 37°C, and a ×100 N.A. 1.4 oil objective. Sequences of images of fluorescent microtubules in cells were captured by using an Andor iXon dv887bf electron multiplying CCD or a Hamamatsu C7190-21 electron bombardment CCD camera controlled by MetaMorph software (Molecular Devices). To minimize background fluorescence, cells were imaged in Hanks's balanced salt solution (Invitrogen) supplemented with 10 mg/ml BSA (Sigma). Microtubule growth trajectories were altered by applying a local force to cells with Femtotip microneedles controlled with a micromanipulator (Eppendorf, Westbury, NY).

Image Analysis. Microtubule contours were analyzed with an automated image analysis algorithm written in IDL and described in detail elsewhere (8). Briefly, the position coordinates of the microtubules were extracted from each image with subpixel accuracy (20 nm or 0.15 pixels) by thresholding, skeletonization, and subsequent position refinement from fits of Gaussian intensity profiles along perpendicular cuts across the filament. To track microtubules in the dense cytoskeleton of living cells, we extended the tracking algorithm with a graphical interface. The Fourier amplitudes of the microtubule contour were determined as described in ref. 2. The variance of the instantaneous Fourier amplitudes from ensembles of ≈200 microtubules in fixed cells was determined by binning data according to wave vector into bins of size ≈0.1 μm^{-1} and subsequently determining the variance by direct calculation or from the variance of a Gaussian fit to the distribution of amplitudes, the latter helping to avoid errors associated with occasional filament misidentification. For the time-dependent fluctuations of the Fourier amplitudes of individual GFP-microtubule, data from ≈20 filaments was averaged by using Origin (OriginLab). To track the tips of microtubules in YFP CLIP-170 CHO cells, we processed images using a Gaussian bandpass filter and then determined tip location using an intensity-weighted center-of-mass tracking algorithm (20). For Fourier analysis of these tracks, an evenly sampled track contour was first obtained by a local average over tip locations. The variance of the ensemble of Fourier amplitudes was then analyzed as described for the instantaneous Fourier amplitudes of microtubules.

We thank T. J. Mitchison, D. J. Needleman, M. L. Gardel, and G. H. Koenderink for helpful discussions. This work was supported by National Science Foundation Grants DMR-0602684 and CTS-0505929, Harvard Materials Research Science and Engineering Center Grant DMR-0213805, and Harvard Interdisciplinary Graduate Education and Research Training on Biomechanics Grant DGE-0221682. F.C.M. was partially supported by the Foundation for Fundamental Research on Matter. C.P.B. acknowledges the hospitality of Vrije Universiteit.

1. Mitchison T, Kirschner M (1984) *Nature* 312:237–242.
2. Gittes F, Mickey B, Nettleton J, Howard J (1993) *J Cell Biol* 120:923–934.
3. Waterman-Storer CM, Salmon ED (1997) *J Cell Biol* 139:417–434.
4. Odde DJ, Ma L, Briggs AH, Demarco A, Kirschner MW (1999) *J Cell Sci* 112:3283–3288.
5. Brangwynne CP, MacKintosh FC, Kumar S, Geisse NA, Talbot J, Mahadevan L, Parker KK, Ingber DE, Weitz DA (2006) *J Cell Biol* 173:733–741.
6. Kaverina I, Rottner K, Small JV (1998) *J Cell Biol* 142:181–190.
7. Howard J, Hyman AA (2003) *Nature* 422:753–758.
8. Brangwynne CP, Koenderink GH, Barry E, Dogic Z, MacKintosh FC, Weitz DA (2007) *Biophys J* 93:346–359.
9. Schulze E, Kirschner M (1986) *J Cell Biol* 102:1020–1031.
10. Bursac P, Lenormand G, Fabry B, Oliver M, Weitz DA, Viasnoff V, Butler JP, Fredberg JJ (2005) *Nat Mater* 4:557–561.
11. Lau AWC, Hoffman BD, Davies A, Crocker JC, Lubensky TC (2003) *Phys Rev Lett* 91:198101.
12. Mizuno D, Tardin C, Schmidt CF, Mackintosh FC (2007) *Science* 315:370–373.
13. Komarova YA, Vorobjev IA, Borisy GG (2002) *J Cell Sci* 115:3527–3539.
14. Kirschner M, Mitchison T (1986) *Cell* 45:329–342.
15. Felgner H, Frank R, Biernat J, Mandelkow E-M, Madelkow E, Ludin B, Matus A, Schliwa M (1997) *J Cell Biol* 138:1067–1075.
16. Janson ME, Dogterom M (2004) *Biophys J* 87:2723–2736.
17. Dogterom M, Yurke B (1997) *Science* 278:856–860.
18. Peskin CS, Odell GM, Oster GF (1993) *Biophys J* 65:316–324.
19. Mogilner A, Oster G (1996) *Biophys J* 71:3030–3045.
20. Crocker JC, Grier D (1996) *J Colloid Interface Sci* 179:298–310.